JCTC Journal of Chemical Theory and Computation

Modeling the Excited States of Biological Chromophores within Many-Body Green's Function Theory

Yuchen Ma,*,† Michael Rohlfing,† and Carla Molteni‡

Fachbereich Physik, Universität Osnabrück, D-49069 Osnabrück, Germany, and Physics Department, King's College London, Strand, London WC2R 2LS, United Kingdom

Received October 6, 2009

Abstract: First-principle many-body Green's function theory (MBGFT) has been successfully used to describe electronic excitations in many materials, from bulk crystals to nanoparticles. Here we assess its performance for the calculations of the excited states of biological chromophores. MBGFT is based on a set of Green's function equations, whose key ingredients are the electron's self-energy Σ, which is obtained by Hedin's GW approach, and the electron−hole interaction, which is described by the Bethe−Salpeter equation (BSE). The GW approach and the BSE predict orbital energies and excitation energies with high accuracy, respectively. We have calculated the low-lying excited states of a series of model biological chromophores, related to the photoactive yellow protein (PYP), rhodopsin, and the green fluorescent protein (GFP), obtaining a very good agreement with the available experimental and accurate theoretical data; the order of the excited states is also correctly predicted. MBGFT bridges the gap between time-dependent density functional theory and high-level quantum chemistry methods, combining the efficiency of the former with the accuracy of the latter: this makes MBGFT a promising method for studying excitations in complex biological systems.

I. Introduction

The photoactive yellow protein (PYP) and rhodopsin are photoreceptors that transform light into biological signals. Their photocycles are initiated by the photoinduced trans/cis isomerization of their chromophores, which leads to successive conformational changes of the overall protein structure and ultimately produces the biological response.[1] PYP was first found in the halophilic purple bacterium *Ectothiorhodospira halophila* and is linked to the negative phototaxis to blue light; the chromophore of PYP is a deprotonated *p*-coumaric acid (*p*CA), linked to a cysteine in the protein via a thioester bond. The chromophore of rhodopsin is retinal in the protonated Schiff base form; light absorption induces isomerization of 11-*cis*-retinal to all-*trans*-retinal and initiates the visual cycle. The green fluorescent protein (GFP) was first isolated in the jellyfish *Aequorea victoria*; its chromophore is *p*-hydroxybenzylideneimidazolinone (*p*-HBDI)[2] in its neutral or anionic form. GFP is widely used as a biological label, since it can be implanted into host proteins without affecting their normal properties; the host proteins, however, become fluorescent and can be detected in living cells and organisms.

Understanding the photochemical processes in photoactive proteins has attracted much interest in both experiments and theory. A wealth of work has been accomplished to investigate optical spectra, the isomerization processes of chromophores, and the role of solution and protein environment in the electronic excitations. Recent measurements of the optical absorption of chromophores in the gas phase provide an experimental benchmark for theoretical methods.[3−10]

Ab initio calculations for biological chromophores have been performed extensively at various levels of quantum chemistry theory. The methods used include time-dependent density functional theory (TDDFT),[4,6,11−14] second-order approximate coupled cluster singles and doubles model (CC2),[15,16] equation of motion coupled cluster theory (EOM-CCSD),[4,5,13,15,17,18] complete active space with second-order perturbation theory (CASPT2),[18−22] and the augmented

* Corresponding author e-mail: yuma@uos.de.
† Universität Osnabrück.
‡ King's College London.

10.1021/ct900528h
Published on Web 11/02/2009

version of the multiconfigurational quasi-degenerate perturbation theory (aug-MCQDPT2):[10,23] both accuracy and computational cost progressively increase from TDDFT, through CC2, EOM-CCSD, CASPT2 up to aug-MCQDPT2. Recently quantum Monte Carlo has also been used for evaluating excited states.[24,25]

Semiempirical methods, like ZINDO, also can give good approximations for the excited states of biological chromophores at a reduced computational cost,[14] but they might be less transferable to a wide range of systems than ab initio methods.

In spite of many efforts, the accurate calculation of the excited states in relative large molecules remains a challenge. In fact, highly reliable methods such as EOM-CCSD, CASPT2, and aug-MCQDPT2 can only be applied to small systems because of their large computational cost. In the last 2 decades, CASPT2 has been regarded as the standard ab initio method for calculating accurate excited-state properties of organic molecules;[26] however, the quality of CASPT2 excitation energies decreases if the complete active space self-consistent field (CASSCF) function is not a good reference and/or the basis set is not sufficiently large.[27] The average accuracy of EOM-CCSD is generally considered to be of 0.2−0.4 eV.[28,29] As an approximation to CCSD, the typical error in CC2 is within the range of 0.3−0.5 eV.[28,29] EOM-CCSD and CC2 can get good results for singlet excited states that are dominated by single-electron transitions.[26] Recent aug-MCQDPT2 calculations provided very good estimations (within 0.1 eV) for the lowest $\pi \rightarrow \pi^*$ excited state of some chromophore models;[23,27,30] however, the general performance of aug-MCQDPT2 for other excited states is still unknown, which prevents a systematic comparison with other quantum chemistry approaches. TDDFT is the fastest quantum chemistry method for calculating excited states of medium- and large-sized molecules of up to 200 second-row atoms. However, with the commonly used approximations, TDDFT yields substantial errors for excited states of molecules with extended π-systems, as well as for nonlocal electronic transitions such as charge-transfer excitations and excited states with little single-excitation character.[11,31,32] The order of the states and the oscillation strengths are also important factors to test the reliability of a method: at present there is no consensus on these for PYP chromophores, for example.[5] In summary, the applicability of quantum chemistry approaches depends strongly on the system under investigation.

In response to the limitations of traditional quantum chemistry methods, here we propose and test the use of many-body Green's function theory (MBGFT)[33−35] for the study of biological chromophores. We demonstrate that MBGFT can compute accurate excitation energies for chromophores that are in excellent agreement with experiments with a reasonable computational cost. MBGFT is well-known in the physics and materials science community to predict orbital and excitation energies with high accuracy. It has been widely and successfully used for describing optical excitations in many systems, including bulk crystals,[36−38] clusters,[39] polymers,[40,41] inorganic molecules (e.g., SiH_4,[39] CO,[42] NH_3[42]) and organic molecules[40,43] (e.g., benzene and naphthalene). The typical error for the excitation energies is within 0.1−0.2 eV.

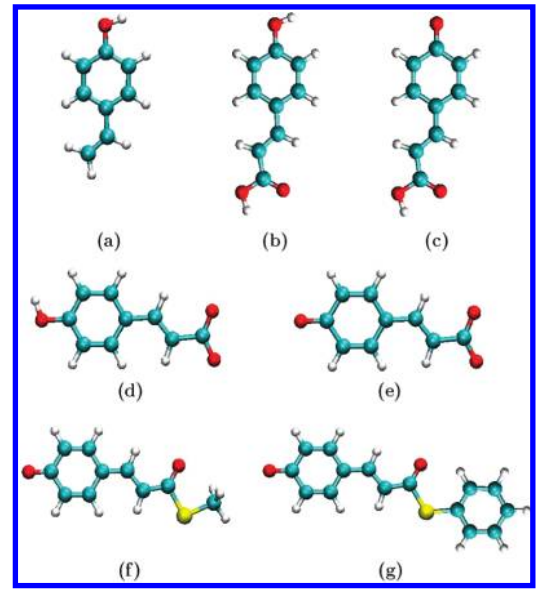

Figure 1. PYP chromophore models studied in this work: (a) *p*VP, (b) *p*CA, (c) *p*CA$^{-\prime}$, (d) *p*CA$^{-\prime\prime}$, (e) *p*CA^{2-}, (f) TMpCA$^-$, and (g) *p*CT$^-$. Carbon, hydrogen, oxygen, and sulfur atoms are represented in cyan, gray, red, and yellow, respectively.

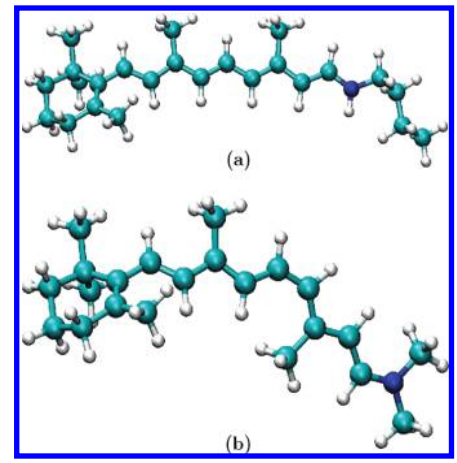

Figure 2. Retinal chromophore models studied in this work: (a) all-trans protonated Shiff base of retinal (PSBT); (b) 11-cis protonated Schiff base of retinal (PSB11).

Here, we present the calculations of the excitation energies of several chromophore models related to PYP, rhodopsin, and GFP, for which experimental data are available, to test the applicability of MBGFT method for biological chromophores. To the best of our knowledge, this work is the first that applies MBGFT method to biological chromophores.

II. Chromophore Models

The 12 chromophore models studied in this work are shown in Figure 1 (PYP chromophore models), Figure 2 (rhodopsin chromophore models), and Figure 3 (GFP chromophore models).

Optical absorption spectra have been measured for the chromophore models related to PYP: *p*-coumaric acid

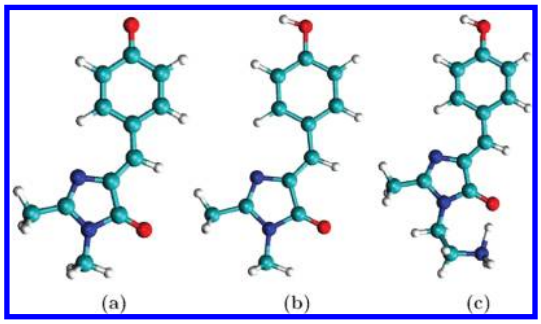

Figure 3. GFP chromophore models studied in this work: (a) *p*-HBDI$^-$, (b) *p*-HBDI, and (c) *p*-HBDI$^+$. Nitrogen atoms are represented in blue.

(*p*CA),[44] the methyloxy ester of *p*CA (OMpCA),[5] deprotonated *p*-coumaric acid (*p*CA$^-$),[8,10,44] the double-anionic form of *p*-coumaric acid (*p*CA^{2-}),[8,44] deprotonated thiomethyl *p*-coumaric acid (TMpCA$^-$)[20] and deprotonated thiophenyl *p*-coumarate (*p*CT$^-$);[8] the chromophore modes of rhodopsin: all-trans protonated Schiff base of retinal (PSBT)[3,9] and 11-cis protonated Schiff base of retinal (PSB11);[9] and the GFP chromophore *p*-HBDI in different charged states (anionic *p*-HBDI$^-$,[7] neutral *p*-HBDI[45]) plus a cationic form of the GFP chromophore,[6] which we simply denote here as *p*-HBDI$^+$, shown in Figure 3c.

For *p*CA$^-$ the deprotonation can occur either at the phenol site or at the carboxyl site as shown in Figure 1c and d, respectively; we denote the two cases as *p*CA$^{-\prime}$ and *p*CA$^{-\prime\prime}$, respectively. The absorption spectrum of *p*-vinylphenol (*p*VP), formed from *p*CA by thermal decarboxylation during the experiment, is also available.[4,46]

III. Methods and Computational Details

The ground-state geometries of the chromophore models are optimized within density functional theory (DFT) using the SIESTA code,[47] employing the PBE generalized gradient approximation (GGA)[48] for the exchange and correlation energy and norm-conserving Troullier−Martins pseudopotentials[49] to describe the interaction between the ion cores and the valence electrons. A double-ζ plus polarization (DZP) basis set made of atomic orbitals is used for the geometry optimization and gives converged structures. In fact, bond length differences between DZP basis set and a larger triple-ζ plus polarization basis set are smaller than 0.004 Å. The PBE exchange and correlation functional is widely used for materials and chemical systems. In comparison with results obtained with other popular functionals, e.g., BLYP[25] and the hybrid B3LYP,[17,50−52] the bond lengths calculated with PBE are on average longer by about 0.01−0.02 Å. Such differences in geometry influence the MBGFT excitation energy by less than 0.1 eV, which makes PBE geometries a reasonable starting point for excitation energy calculation within MBGFT. However, the influence of the DFT exchange-correlation functional on the MBGFT excitation energies deserves further studies.

The excited states of the ground-state geometries obtained as described above are then calculated within MBGFT. At variance from the geometry optimization where basis sets constructed by atomic orbitals were used, the basis set for all steps of the MBGFT calculations is made by atom-centered Gaussian orbitals which have the form

$$\phi_{ijk}(\mathbf{r}) = A_{ijk} x^i y^j z^k \mathrm{e}^{-\alpha r^2} \quad (1)$$

The same exchange and correlation functional and pseudopotentials are used. Four decay constants (α) are used for C, N, O, and S atoms (0.2, 0.5, 1.25, and 3.2 in atomic units (a_0^{-2})), whereas three decay constants are used for H atoms (0.1, 0.4, and 1.5 in atomic units). Gaussian orbitals with s, p, d, and s* symmetry are included for each atom. The number of Gaussian orbitals for each atom is 40 for C, N, O, S and 30 for H, respectively. The decay constants have been tested to give converged orbital and excitation energies. They are adjusted so that orbital energies calculated by the Gaussian orbital basis set reproduce (within 0.1 eV) those obtained by a well-converged plane-wave basis set. A larger basis set, which, besides the atom-centered Gaussian orbitals discussed above, contains additional Gaussian orbitals centered above and below the plane of the molecule to give a better description of the π and π^* orbitals, modifies the lowest excitation energy of *p*CA$^-$ by only 0.03 eV. This shows that the basis set with only atom-centered Gaussian orbitals is able to give converged excitation energies and is suitable to study the selected chromophore models.

In DFT, one needs to solve the Kohn−Sham equation

$$\left\{-\frac{\hbar^2}{2m}\nabla^2 + V_{\mathrm{ps}}(\mathbf{r}) + V_{\mathrm{H}}(\mathbf{r}) + V_{\mathrm{xc}}(\mathbf{r})\right\}\psi_n^{\mathrm{DFT}}(\mathbf{r}) = E_n^{\mathrm{DFT}}\psi_n^{\mathrm{DFT}}(\mathbf{r}) \quad (2)$$

where V_{ps} and V_{H} are the pseudopotentials describing the electron−ion interaction and the Hartree potential, respectively, and V_{xc} is the exchange-correlation potential. Approximation to the exchange-correlation potential in DFT makes it fail to predict correctly the orbital energies. In MBGFT, accurate orbital energies can be obtained within the GW approximation (GWA), proposed by Hedin and Lundqvist.[33] An accurate prediction of the orbital energies is an essential prerequisite for the further excited-state calculation in MBGFT. GWA has been successfully applied to compute band structures of a large number of solids[53] and orbital energies of many molecules[42,43] including organic molecules.[43] Within GWA, V_{xc} in DFT is replaced by a nonlocal, energy-dependent self-energy operator $\Sigma(\mathbf{r}, \mathbf{r}', E)$, which fulfills the GW equation[54]

$$\left\{-\frac{\hbar^2}{2m}\nabla^2 + V_{\mathrm{ps}}(\mathbf{r}) + V_{\mathrm{H}}(\mathbf{r})\right\}\psi_n^{\mathrm{GWA}}(\mathbf{r}) + \int \Sigma(\mathbf{r}, \mathbf{r}', E_n^{\mathrm{GWA}})\psi_n^{\mathrm{GWA}}(\mathbf{r}')\,\mathrm{d}\mathbf{r}' = E_n^{\mathrm{GWA}}\psi_n^{\mathrm{GWA}}(\mathbf{r}) \quad (3)$$

The self-energy operator $\Sigma(\mathbf{r}, \mathbf{r}', E)$ can be evaluated by

$$\Sigma(\mathbf{r}, \mathbf{r}', E) = \frac{\mathrm{i}}{2\pi}\int \mathrm{e}^{-\mathrm{i}\omega 0^+} G(\mathbf{r}, \mathbf{r}', E - \omega) W(\mathbf{r}, \mathbf{r}', \omega)\,\mathrm{d}\omega \quad (4)$$

where G and W are the one-body Green function and the dynamically screened Coulomb interaction, respectively. G and W are in the forms

$$G(\mathbf{r},\mathbf{r}',E) = \sum_n \frac{\psi_n(\mathbf{r})\psi_n^*(\mathbf{r}')}{E - E_n + \mathrm{i}0^+ \,\mathrm{sgn}(E_n - \mu)} \quad (5)$$

and

$$W = \varepsilon^{-1} v \quad (6)$$

respectively, where ε and v are the dielectric function and the bare Coulomb interaction, respectively. μ is the chemical potential. G and W are evaluated based on the ground-state wave functions and energies obtained from eq 2. ε is calculated within the random-phase approximation.[54] Usually, the GWA orbital energies are evaluated perturbatively to first order by

$$E_n^{\mathrm{GWA}} = E_n^{\mathrm{DFT}} + Z_n\langle\psi_n^{\mathrm{DFT}}|\Sigma(E_n^{\mathrm{DFT}}) - V_{\mathrm{xc}}|\psi_n^{\mathrm{DFT}}\rangle \quad (7)$$

based on the assumption that the DFT wave function in eq 2 agrees well with the GWA wave function in eq 3 in most cases.[56] Z_n is the renormalization constant to take into account the energy dependence of the self-energy[56]

$$Z_n = 1 - \left[\left.\frac{\partial\Sigma_n(E)}{\partial E}\right|_{E=E_n^{\mathrm{GWA}}}\right]^{-1} \quad (8)$$

where $\Sigma_n(E) = \langle\psi_n^{\mathrm{DFT}}|\Sigma(E)|\psi_n^{\mathrm{DFT}}\rangle$.

By applying GWA, the original occupied orbitals within DFT are shifted down while the unoccupied orbitals are raised up, as shown in Figure 4 and discussed in the following section for *p*CA and *p*CA$^{-\prime}$. In some cases the order of energy levels may change from DFT to GWA; for example, in *p*CA HOMO − 1 in DFT becomes HOMO − 2 in GWA, while HOMO − 2 in DFT turns out to be HOMO − 1 in GWA.

If an electron is excited into a higher state it leaves a hole in its old state. The excited electron and the hole cannot be treated separately, since the electron feels the presence of the hole. Due to the Coulomb interaction between the excited electrons and holes, optical electron−hole excitations cannot be described by an effective one-particle picture. Instead, it is necessary to consider two-particle (electron and hole) states which can be described as

$$\chi(\mathbf{r}_e,\mathbf{r}_h) = \sum_{\alpha}^{\mathrm{occ}}\sum_{\beta}^{\mathrm{virt}} [A_{\alpha\beta}\psi_\beta(\mathbf{r}_e)\psi_\alpha^*(\mathbf{r}_h) + B_{\alpha\beta}\psi_\alpha(\mathbf{r}_e)\psi_\beta^*(\mathbf{r}_h)] \quad (9)$$

where $A_{\alpha\beta}$ and $B_{\alpha\beta}$ are resonant (occupied → virtual) and antiresonant (virtual → occupied) electron−hole amplitudes, respectively, and α and β denote the one-particle occupied and virtual orbitals, respectively. The motion of the electron−hole pair, well-represented by the two-particle Green's function, can be rigorously described by the Bethe−Salpeter equation (BSE).[34,35] For singlet-to-singlet excitations, the generalized BSE takes the form[34]

$$\begin{pmatrix} R & C \\ -C^* & -R^* \end{pmatrix}\begin{pmatrix} A \\ B \end{pmatrix} = \Omega\begin{pmatrix} A \\ B \end{pmatrix} \quad (10)$$

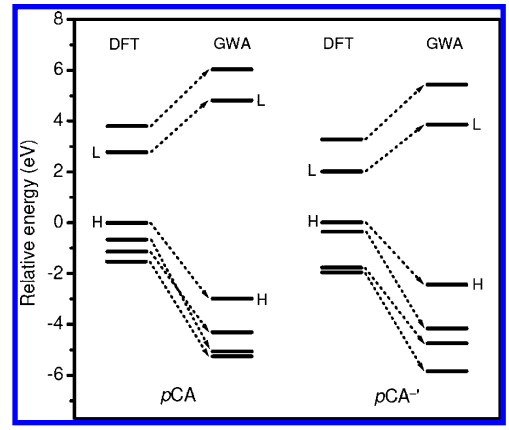

Figure 4. Energy levels (four occupied and two unoccupied) of *p*CA and *p*CA$^{-\prime}$ calculated within DFT and GWA. H and L denote the highest occupied molecular orbital (HOMO) and lowest unoccupied molecular orbital (LUMO), respectively. The energy levels in DFT and the corresponding ones in GWA are connected by dotted arrow lines. In both chromophore models, the energies of the highest occupied orbitals (H) within DFT are set to zero.

with $R = D + 2K^{R,x} + K^{R,d}$, $C = 2K^{C,x} + K^{C,d}$, and $D = E_{\mathrm{occ}}^{\mathrm{GWA}} - E_{\mathrm{virt}}^{\mathrm{GWA}}$.[35] R and $-R^*$ are the Hamiltonians corresponding to the resonant and antiresonant parts of the transitions, respectively, whereas C and $-C^*$ are the coupling terms between resonant and antiresonant transitions. D is the free interlevel transition energy between occupied and virtual orbitals. Ω is the excitation energy, i.e., the energy difference between the excited state and the ground state within the Franck−Condon approximation. $K^{R,x}$ ($K^{R,d}$) is the bare exchange term (screened direct term) of the electron−hole interaction kernel for the resonant transition, whereas $K^{C,x}$ ($K^{C,d}$) are corresponding terms for the coupling terms.

The procedure to compute the optical spectrum with MBGFT is that first, conventional DFT (here within PBE-GGA) is performed to calculate the ground-state orbital energies and wave functions; then, accurate orbital energies are computed within GWA with the ground-state orbital energies and wave functions as input parameters; finally, BSE is solved with the GWA orbital energies and ground-state wave functions (used to construct the excited state in eq 9) as input parameters. Indicatively, a GW + BSE calculation for one of the chromophore models studied in this work can usually be completed within half a day with a single CPU.

MBGFT calculations of the excitation energies for crystals, clusters, nanotubes, and polymers are usually done within Tamm−Dancoff approximation (TDA),[34] i.e., the coupling term C in eq 10 is omitted. The coupling term C is in fact nearly zero for these systems, and TDA only influences the excitation energy by about 0.1 eV. However, for the chromophores studied here, we find that the magnitude of the coupling term C is comparable to that of the resonant transition R in eq 10 so that the coupling term cannot be neglected, and we have to solve the full BSE. TDA only influences the excitation energy related to the $\pi \rightarrow \pi^*$ transitions. For example, for the lowest $\pi \rightarrow \pi^*$ transitions in all the chromophore models, TDA overestimates the excitation energy by at least 0.4 eV. In contrast, TDA has very weak influence on the energy for the $n \rightarrow \pi^*$ excitations.

Table 1. Selected Excitation Energies (in eV) of PYP, GFP, and Retinal Chromophore Models Calculated by Many-Body Green's Function Theory and Their Comparison with Reference Experimental Data and a Selection of Theoretical Values[a]

model	experiment	MBGFT		other theory
*p*VP	4.12 (ref 4)	S_1	4.17	4.19 (ref 4)[b], 4.57 (ref 11)[c], 4.66 (ref 4)[d]
	4.75 (ref 4)	S_2	4.60	4.52 (ref 4)[b], 5.43 (ref 4)[d]
*p*CA	4.06 (ref 5)[e], 4.00 (ref 44)[f]	S_1	3.94	3.78 (ref 12)[g], 4.15 (ref 5)[h], 4.20 (ref 11)[c], 4.69 (ref 5)[d], 4.92 (ref 17)[i]
	4.37 (ref 5)[e]	S_2	4.20	4.58 (ref 5)[h], 4.95 (ref 5)[d], 5.14 (ref 17)[i], 5.22 (ref 12)[g]
$pCA^{-\prime}$	2.88 (refs 8, 10)	S_1	2.95	2.79 (ref 10)[j], 2.82 (ref 10)[k], 3.10 (ref 10)[l], 3.24 (ref 12)[g], 3.40 (ref 10)[m]
$pCA^{-\prime\prime}$	4.36 (ref 8)[f], 4.39 (ref 44)[f]	S_4	4.37	2.85 (ref 30)[k], 4.70 (ref 10)[m], 4.79 (ref 10)[l], 5.17 (ref 27)[j]
pCA^{2-}	3.69 (ref 8)[f], 3.72 (ref 44)[f]	S_2	3.73	
$TMpCA^-$	2.78 (ref 20)[n]	S_1	2.80	2.58 (ref 20)[o], 2.89 (ref 15)[p], 3.18 (ref 15)[q], 3.32 (ref 11)[c]
pCT^-	2.70 (ref 8)	S_1	2.75	2.71 (ref 30)[k], 3.01 (ref 12)[g], 3.05 (ref 11)[c]
p-$HBDI^-$	2.59 (ref 7)	S_1	2.67	2.52 (ref 30)[r], 2.66 (ref 18)[s,t], 2.92 (ref 25)[u], 3.12 (ref 18)[s,v], 2.93 (ref 25)[w], 3.04 (ref 25)[x]
p-HBDI	3.12 (ref 45)[n]	S_1	3.17	3.46 (ref 6)[y], 3.85 (ref 18)[s,t], 3.58 (ref 25)[u], 4.21 (ref 18)[s,v], 3.20 (ref 25)[w]
p-$HBDI^+$	2.99 (ref 6)	S_1	2.93	3.34 (ref 6)[y], 3.21 (ref 25)[u], 3.21 (ref 25)[w], 3.36 (ref 25)[x]
PSBT	2.00 (ref 9), 2.03 (ref 3)	S_1	2.09	2.03 (ref 30)[z], 2.07 (ref 22)[aa], 2.28 (ref 51)[ab], 2.32 (ref 19)[ac]
	3.22 (ref 9)	S_2	3.10	2.85 (ref 22)[aa], 3.12 (ref 51)[ab], 3.51 (ref 19)[ac]
PSB11	2.03 (ref 9)	S_1	2.04	2.07 (ref 23)[z], 2.05 (ref 22)[aa], 2.27 (ref 51)[ab], 2.32 (ref 19)[ac], 2.14 (ref 16)[ad]
	3.18 (ref 9)	S_2	3.01	2.84 (ref 22)[aa], 3.10 (ref 51)[ab], 3.49 (ref 19)[ac], 3.21 (ref 16)[ad]

[a] Details of the theoretical methodologies and basis sets used for the calculation of the excited-state energies//ground-state geometries for the theoretical results are given. [b] TDDFT(BP86)/def-TZVP//DFT(BP86)/def-TZVP. [c] TDDFT(B3LYP)/cc-PVTZ//DFT(B3LYP)/cc-PVTZ. [d] EOM-CCSD/6-31+G*//CCSD/cc-pVDZ. [e] OMpCA. [f] In solution. [g] TDDFT(BP86)/TZP//DFT(BP86)/PW. [h] TDDFT(B3LYP)/def-TZVP//DFT(B3LYP)/def-TZVP. [i] EOM-CCSD/6-31G*//DFT(B3LYP)/6-31G**. [j] MRMP2/CASSCF(14,12)/(p-type d-aug)-cc-pVDZ//DFT(PBE0)/cc-pVDZ. [k] aug-MCQDPT2/CASSCF(14,12)/(p-type d-aug)-cc-pVDZ//DFT(PBE0)/cc-pVDZ. [l] RI-CC2/aug-cc-pVTZ//DFT(PBE0)/aug-cc-pVDZ. [m] TDDFT(CAM-B3LYP)/aug-cc-pVTZ//DFT(PBE0)/aug-cc-pVDZ. [n] In the protein. [o] MS-CASPT2/CASSCF(12,10)/ANO//CASSCF(12,10)/ANO. [p] CC2/SV(P)//HF/6-31G*. [q] EOM-CCSD/6-31G*//HF/6-31G*. [r] aug-MCQDPT2/CASSCF(16,14)/(p-type d-aug)-cc-pVDZ//DFT(PBE0)/cc-pVDZ. [s] A 2,3-dimethyl model. [t] SA-2-CAS(2,2)PT2/6-31G//SA-2-CAS(2,2)/6-31G. [u] CASPT2/CASSCF(14,14)/cc-pVDZ//DFT(BLYP)/cc-pVTZ. [v] EOM-CCSD/6-31G//SA-2-CAS(2,2)/6-31G. [w] TDDFT(SAOP)/ET-pVQZ//DFT(BLYP)/cc-pVTZ. [x] Diffusion Quantum Monte Carlo/cc-pVDZ//DFT(BLYP)/cc-pVTZ. [y] TDDFT(B3LYP)/6-311++G*//MP3. [z] aug-MCQDPT2/CASSCF(12,12)/(p-type d-aug)-cc-pVDZ//DFT(PBE0)/cc-pVDZ. [aa] CASPT2/CASSCF(12,12)/ANO//MP2/6-31G**. [ab] TDDFT(B3LYP)/6-311++G(d)//DFT(B3LYP)/6-31G(d). [ac] CASPT2/CASSCF(12,12)/6-31G*//CASSCF(12,12)/6-31G*. [ad] CC2/def2-TZVPP//MP2/TZVP.

Chromophores are quasi-zero-dimensional systems. The distribution of the excited electron and the hole is highly localized. It is the huge exchange interaction between the excited electron and the hole that makes the resonant−anti-resonant coupling not negligible. When the dimension of the system increases, such as in polymers, nanotubes, and bulk solids, the excited electron and hole becomes delocalized and the influence of TDA decreases gradually.

We also include dynamical screening effects in the electron−hole interaction. In comparison to the results from calculations with only static screening, we find that the influence of dynamical screening on the excitation energies is about 0.1 eV for the lowest $\pi \rightarrow \pi^*$ transitions, but for the lowest $n \rightarrow \pi^*$ transitions the influence is larger, up to 0.25 eV.

IV. Results and Discussion

IV.A. Neutral PYP Chromophores. Ryan et al.[46] tried to measure the gas-phase optical absorption spectrum of *p*CA. However, de Groot and Buma[55] pointed out that the spectrum obtained should be attributed to *p*VP due to the decarboxylation of *p*CA in the experiment, which is proved by the excitation spectrum measurement on *p*VP itself.[4,55] The excitation spectrum of the methyloxy ester of *p*CA (OMpCA), with the hydrogen atom at the carboxyl group replaced by a methyl group, was recently obtained by de Groot et al.[5] EOM-CCSD calculations indicate that the influence of the methyl substituent on the excitation energies is very small,[5] which is also confirmed by our MBGFT calculations. So the excitation energies from the OMpCA spectrum could be regarded as a good reference for those in *p*CA. The absorption spectrum of *p*CA was also measured by Putschögl et al.[44] in pH 1 aqueous solution, which gave the first absorption peak in energy close to that of the gas-phase OMpCA.

MBGFT gives excitation energies in good agreement with experiments for *p*VP and *p*CA, with discrepancy within 0.1 eV (10 nm) and 0.2 eV (20 nm) for the first (S_1) and second (S_2) excited states, respectively, as shown in Table 1.

The characters of the excitations are still an open question for *p*CA. For example, most of the TDDFT, EOM-CCSD, and CASPT2 calculations[5,12,17,50] showed that S_1 and S_2 are $\pi \rightarrow \pi^*$ states and S_3 is an $n \rightarrow \pi^*$ state, whereas the CASPT2 calculation by Li and Fang[57] predicted that S_1 is an $n \rightarrow \pi^*$ state and S_2 is a $\pi \rightarrow \pi^*$ state. On the basis of EOM-CCSD,[5,50] S_1 originates from the HOMO → LUMO + 1 transition, whereas S_2 has a dominant contribution from the HOMO → LUMO transition.

According to the MBGFT calculations, S_1 and S_2 are $\pi \rightarrow \pi^*$ states and S_3 is an $n \rightarrow \pi^*$ state with the excitation energy of 3.94, 4.20. and 4.30 eV, respectively. The oscillator strength of S_1 is larger than that of S_2. In DFT within PBE-GGA, HOMO − 2, HOMO, LUMO, and LUMO + 1 are π states, whereas HOMO − 1 is an *n* state. In GWA, which gives more accurate orbital energies, the order between HOMO − 1 and HOMO − 2 is interchanged as shown in

Figure 4, with HOMO − 2 the *n* state and HOMO − 1 the π state. S_3 originates from HOMO − 2 → LUMO transition (in this context, when discussing results obtained within MBGFT, orbitals are in the order computed within GWA). Both S_1 and S_2 contain contributions from HOMO → LUMO, HOMO → LUMO + 1, and HOMO − 1 → LUMO transitions, with HOMO → LUMO and HOMO → LUMO + 1 dominating S_1 and S_2, respectively.

For *p*VP, both MBGFT and EOM-CCSD[4] predict a much smaller oscillator strength for S_1 than S_2, which is in agreement with experiment.[4] S_1 and S_2 are dominated by HOMO → LUMO + 1 and HOMO → LUMO transitions, respectively, according to both methods.

IV.B. Anionic PYP Chromophores. *IV.B.1. pCA^- and pCA^{2-}.* Electrospray ionization (ESI) is routinely used to produce gas-phase compounds, including PYP chromophores,[8] retinal chromophores,[3,9] and tyrosine.[58,59] Most of these species, such as *p*CA and tyrosine, have more than one acidic site, so the structure produced in electrospray technique is unclear. For *p*CA the carboxylic acid site is more acidic than the phenolic one in solution, so the gas-phase absorption spectrum of pCA^- was originally attributed to the model $pCA^{-\prime\prime}$,[8,30] as illustrated in Figure 1d in which the carboxylic group is deprotonated, similarly to the case in solution. Recent experiments on tyrosine[58,59] find that deprotonation in the gas phase occurs preferentially at the phenolic site if the compound was sprayed from a methanol solution through ESI. The gas-phase pCA^- used in the experiment was also produced from a methanol solution,[8] which makes the assignment of the absorption peak at 430 nm (2.88 eV) to $pCA^{-\prime\prime}$ questionable. In neutral aqueous solution, pCA^- preferentially exists in the form of $pCA^{-\prime\prime}$ as discussed above, so the absorption peak of $pCA^{-\prime\prime}$ in aqueous solution can be determined to be around 4.36 eV, according to the experiments performed by Nielsen et al.[8] and Putschögl et al.[44] In alkaline aqueous solution, $pCA^{-\prime\prime}$ transforms to pCA^{2-}, which was observed to have an absorption maximum around 3.70 eV.[8,44] Very recently pCA^- was also experimentally studied in vacuo, together with two methyl derivatives of it, which allowed for the study of the phenoxide and carboxylate forms.[10] The absorption maximum for all three chromophores was again 430 nm (2.88 eV), suggesting that both the phenoxide and carboxylate forms might have the same absorption properties. However, the analysis of the photodissociation pathways of pCA^- suggested that only the phenoxide isomer was present in a substantial amount, and the presence of $pCA^{-\prime\prime}$ could not be verified.[10] DFT and RI-CC2 calculations also showed that $pCA^{-\prime}$ is more stable than $pCA^{-\prime\prime}$ in vacuo.[10]

According to the MBGFT calculations, the absorption maxima of $pCA^{-\prime}$, $pCA^{-\prime\prime}$, and pCA^{2-} are predicted at 2.95, 4.37, and 3.73 eV, respectively. If the gas-phase absorption peak measured by Nielsen et al.[8] and Rocha-Rinza et al.[10] is attributed to $pCA^{-\prime}$ rather than $pCA^{-\prime\prime}$, our result is in very good agreement with the experiment as shown in Table 1. The absorption maximum in vacuo we obtained for $pCA^{-\prime\prime}$ is very close to those measured in solution.[8,44]

The excitations in $pCA^{-\prime}$ are simple, with S_1 (2.95 eV) dominated by the HOMO → LUMO ($\pi \rightarrow \pi^*$) transition and S_2 (3.32 eV) dominated by the HOMO − 1 → LUMO ($n \rightarrow \pi^*$) transition, with no reordering of the energy levels within GWA as shown in Figure 4. The situation in $pCA^{-\prime\prime}$ is more complex. With DFT within PBE-GGA, HOMO and HOMO − 1 are *n* states, HOMO − 2 and HOMO − 3 are π states, LUMO and LUMO + 2 are π^* states, whereas LUMO + 1 is a Rydberg-type orbital with appreciable electron density beyond the frame of the molecule. Within GWA, the highest four occupied orbitals are reordered, with the original HOMO − 3 in DFT becoming HOMO, while the order of the other three occupied orbitals remains. The energies of the lowest four excited states within MBGFT are calculated to be 3.47, 3.63, 3.87, and 4.37 eV. S_1 and S_2 are $n \rightarrow \pi^*$ excitations mainly induced by transitions from the highest two *n* orbitals to the lowest two π^* orbitals; S_3 and S_4 are $\pi \rightarrow \pi^*$ excitations mainly induced by HOMO → LUMO and HOMO → LUMO + 2 transitions, with S_3 dominated by HOMO → LUMO and S_4 by HOMO → LUMO + 2 transitions. The absorption peak observed in the experiments originates from S_4, which has the strongest oscillator strength.

Within GWA, for pCA^{2-}, HOMO is a π state with electron density mainly localized at the phenolic oxygen, HOMO − 1 and HOMO − 2 are *n* states with electronic density localized on the two carboxylic oxygens, LUMO and LUMO + 2 are π^* orbitals, whereas LUMO + 1 is a Rydberg-type orbital. The lowest two excited states S_1 and S_2 are of $\pi \rightarrow \pi^*$ character, with energies of 3.37 and 3.73 eV, respectively. Both these states have contribution from HOMO → LUMO and HOMO → LUMO + 2 transitions. S_3 and S_4 are $n \rightarrow \pi^*$ excitations, and S_5 is a $\pi \rightarrow$ Rydberg excitation. S_2, with the highest oscillator strength, is responsible for the absorption maximum (∼3.70 eV) observed in experiments.

MRMP2 (multireference second-order Møller−Plesset perturbation theory) and aug-MCQDPT2 have been used to study $pCA^{-\prime\prime}$ by Nemukhin et al.[30] and Andersen and Bochenkova;[27] however, the calculated energies are quite different, 5.17 eV by the former and 2.85 eV by the latter. The results from TDDFT and CC2 are close to that from MRMP2 but deviate from the aug-MCQDPT2 value by around 2.0 eV;[10] MCQDPT2 results support the idea that $pCA^{-\prime}$ and $pCA^{-\prime\prime}$ have very similar absorption properties,[10] whereas all the other theoretical methods, including MBGFT, suggest that $pCA^{-\prime}$ is the isomer present in vacuo; if present in vacuo, $pCA^{-\prime\prime}$ would have an absorption peak similar to that measured in solution.

IV.B.2. TMpCA⁻ and pCT⁻. The optical absorption maximum of pCT^- in vacuo was measured by Nielsen et al. to be 2.70 eV.[8] pCT^- should have similar excitation properties to the chromophore in the protein. Comparison of its absorption maximum in vacuo with that in the protein at 2.78 eV[8,60] shows only a small influence (∼0.08 eV) of the protein environment on the absorption spectrum. Until now, there is no measurement on the absorption spectrum of $TMpCA^-$ in vacuo besides the absorption spectrum in the protein which gives two excitation energies at 2.78 and 3.14 eV,[61] respectively. If the protein effects are small as concluded by Nielsen et al.,[8] these energies could be reasonable references for excitation energies of $TMpCA^-$

in vacuo, which should also not differ substantially from those of pCT$^-$.

The first absorption peaks of pCT$^-$ and TMpCA$^-$ have been attributed to $\pi \rightarrow \pi^*$ excitations. aug-MCQDPT2 obtained this excitation energy in excellent agreement with experiment for pCT$^-$.[30] For TMpCA$^-$, the excitation energies calculated with CC2,[15] EOM-CCSD,[15] and CASPT2[20] deviate from experimental values by 0.1, 0.4, and 0.2 eV, respectively. However, the excitation energy at 2.89 eV by CC2 for TMpCA$^-$ given in Table 1 is the second excited state, with the lowest excited state being an $n \rightarrow \pi^*$ state at the energy of 2.84 eV.[15] The experimental 3.14 eV excitation is thought to initiate an alternative route for PYP excitation photocycle and was considered to involve an excited state different from the lowest $\pi \rightarrow \pi^*$ excitation in TmpCA$^-$.[61] S_2 computed by CASPT2 is an $n \rightarrow \pi^*$ state at the energy of 2.95 eV and is regarded as the origin of the excitation at 3.14 eV observed in the experiment.[20] EOM-CCSD predicts an $n \rightarrow \pi^*$ state as the second excited state with the energy of 3.82 eV, deviating from the experimental value by 0.68 eV.

With MBGFT, the characters of S_1 and S_2 in TMpCA$^-$ and pCT$^-$ are similar to those of S_1 and S_2 in pCA$^{-\prime}$ since the electronic density involved in these two states does not exceed the carboxyl group in both compounds. S_1 is a $\pi \rightarrow \pi^*$ state dominated by the HOMO $\rightarrow$ LUMO transition, whereas S_2 is an $n \rightarrow \pi^*$ state dominated by the HOMO $-$ 1 $\rightarrow$ LUMO transition. The energies of S_1 for TMpCA$^-$ and pCT$^-$ are calculated to be 2.80 and 2.75 eV, respectively, deviating from the experimental values by 0.02 and 0.05 eV, respectively. The energy of S_2 for TMpCA$^-$ is calculated to be 3.19 eV, which is very close to the experimental excitation energy at 3.14 eV. Assuming that the protein effects are small, the agreement with the experiments is excellent.

IV.C. GFP Chromophores. GFP chromophores exhibit two absorption maxima at 3.12 and 2.60 eV in the protein,[7] which are attributed to the neutral (p-HBDI) and anionic (p-HBDI$^-$) forms shown in Figure 3, respectively. The absorption maximum of the neutral form has a weak dependence on the environment, e.g., protein and solvent.[62,63] The excitation energy of the neutral form in vacuo should therefore be very close to 3.12 eV. The absorption maximum of the anionic form in vacuo was measured to be at 2.59 eV,[7] also close to that in the protein, which indicates that the protein environment has little disturbance on the electronic structure of the chromophore.[64] Lammich et al. also measured in vacuo the spectrum of a cationic form of the GFP chromophore shown in Figure 3c, here simply denoted as p-HBDI$^+$, which exhibits an absorption peak at 2.99 eV.[6]

Within MBGFT, the absorption maxima for the neutral, anionic, and cationic forms of GFP chromophore are 3.17, 2.67, and 2.93 eV, deviating from the experimental data by at most 0.07 eV, respectively. All these excitations have HOMO $\rightarrow$ LUMO character.

GFP chromophores models have been theoretically studied with a range of techniques including TDDFT, CASPT2, EOM-CCSD, SOS-CIS(D), MRMP2, aug-MCQDPT2, and quantum Monte Carlo,[6,13,18,21,25,30] and comparison between the results obtained with different methods and approximations has been recently discussed;[13,25] a selection of these results is shown in Table 1.

IV.D. Retinal Chromophores. Successful measurement of the optical absorption spectra of isolated PSBT and PBS11 molecules in vacuo has stimulated a large number of quantum chemistry studies.[16,19,22,23,30] The computational requirement of TDDFT is the least; however, excitation energies calculated through TDDFT depend drastically on the exchange-correlation functional used[51] and they are not accurate.[52] In comparison to experimental values, CASPT2 calculations by Sekharan et al.[22] gave a good results for S_1, but the energies of S_2 was underestimated by 0.3−0.4 eV. Other CASPT2 calculations by Cembran et al.[19] overestimated the energies of both S_1 and S_2 by 0.3 eV. Recent high-level aug-MCQDPT2 calculations predicted good excitation energies for S_1;[23,30] however, its performance on S_2 is unknown. It is somehow surprising that the lower-level CC2 method succeeded in computing energies of both S_1 and S_2 for PSB11[16] with high accuracy, and the origin of this success needs to be further clarified.

With MBGFT, we get excellent S_1 excitation energies for both PSBT and PSB11, with accuracy at the same level as aug-MCQDPT2. The performance of MBGFT on S_2 is also good, with deviation from experimental results by 0.17 eV at most, which is about half the typical error of CASPT2 for S_2. In both PSBT and PSB11, S_1, which has mainly HOMO $\rightarrow$ LUMO character (90%), has an oscillator strength stronger than that of S_2, which has mainly HOMO $-$ 1 $\rightarrow$ LUMO (75%) character complemented by HOMO $\rightarrow$ LUMO $+$ 1 (15%) contribution.

V. Conclusions

In this work, we have applied for the first time MBGFT to the study of the excited states of PYP, rhodopsin, and GFP chromophores. Its performance has been extensively tested on several chromophore models, including both neutral and charged ones. Excellent agreement with the available experiments are obtained for the excitation energies for all the models, with errors within 0.1 eV (10 nm) for the lowest absorption maximum with $\pi \rightarrow \pi^*$ character excitations and $n \rightarrow \pi^*$ excitations, whereas the accuracy for the second $\pi \rightarrow \pi^*$ excitations is within 0.2 eV. The order of the states is also reproduced correctly. More accurate prediction (within an error of 0.1 eV) of the second $\pi \rightarrow \pi^*$ state may require consideration of double excitations,[27] which is beyond the ability of the current MBGF method.

With respect to other theoretical methods, whose applicability depends drastically on the specific chromophore models, MBGFT has the advantages of high accuracy, good transferability, and reasonable computational cost, which become important for relatively large chromophores, like the protonated Schiff base of retinal. An important feature of MBGFT is the possibility to incorporate at minimal cost polarizability and screening effects outside the object under consideration, which may affect the excited states because of nonlocal correlation effects, in terms of the screened Coulomb interaction. This is particularly relevant for biological chromophores, where the protein environment tunes and catalyzes the photoreaction. Moreover, progress in the

calculation of forces in the excited state within MBGFT has recently been made,[42,65] opening the way to the study of isomerization processes and excited-state dynamics. All these features make MBGFT a very promising tool for the investigation of photoactive proteins.

We also find necessary to go beyond the Tamm−Dancoff approximation for the application of MBGFT in chromophores. The influence of the resonant−antiresonant transitions coupling on the absorption maximum is larger than 0.4 eV for chromophores, which is quite different from that in crystals and clusters. This provides guidelines for further applications of MBGFT to similar low-dimensional systems.

Acknowledgment. This work has been supported by the Deutsche Forschungsgemeinschaft (Bonn, Germany) by Grant No. Ro 1318/4-3. Y.M. thanks the London Thomas Young Centre for the Theory and Simulations of Materials for financial support during a collaborative visit to King's College London.

Supporting Information Available: DFT-PBE geometries of the model chromophores. This material is available free of charge via the Internet at http://pubs.acs.org.

References

(1) van der Horst, M. A.; Hellingwerf, K. J. *Acc. Chem. Res.* **2004**, *37*, 13.

(2) Shimomura, O. *FEBS Lett.* **1979**, *104*, 220.

(3) Andersen, L. H.; Nielsen, I. B.; Kristensen, M. B.; El Ghazaly, M. O. A.; Haacke, S.; Brøndsted Nielsen, M.; Åxman Petersen, M. *J. Am. Chem. Soc.* **2005**, *127*, 12347.

(4) de Groot, M.; Buma, W. J.; Gromov, E. V.; Burghardt, I.; Köppel, H.; Cederbaum, L. S. *J. Chem. Phys.* **2006**, *125*, 204303.

(5) de Groot, M.; Gromov, E. V.; Köppel, H.; Buma, W. J. *J. Phys. Chem. B* **2008**, *112*, 4427.

(6) Lammich, L.; Åxman Petersen, M.; Brøndsted Nielsen, M.; Andersen, L. H. *Biophys. J.* **2007**, *92*, 201.

(7) Nielsen, S. B.; Lapierre, A.; Andersen, J. U.; Pedersen, U. V.; Tomita, S.; Andersen, L. H. *Phys. Rev. Lett.* **2001**, *87*, 228102.

(8) Nielsen, I. B.; Boyé-Péronne, S.; El Ghazaly, M. O. A.; Kristensen, M. B.; Brøndsted Nielsen, S.; Andersen, L. H. *Biophys. J.* **2005**, *89*, 2597.

(9) Nielsen, I. B.; Lammich, L.; Andersen, L. H. *Phys. Rev. Lett.* **2006**, *96*, 018304.

(10) Rocha-Rinza, T.; Christiansen, O.; Rajput, J.; Gopalan, A.; Rahbek, D. B.; Andersen, L. H.; Bochenkova, A. V.; Granovsky, A. A.; Bravaya, K. B.; Nemukhin, A. V.; Christiansen, K. L.; Nielsen, M. B. *J. Phys. Chem. A* **2009**, *113*, 9442.

(11) Muguruza González, E.; Guidoni, L.; Molteni, C. *Phys. Chem. Chem. Phys.* **2009**, *11*, 4556.

(12) Sergi, A.; Grüning, M.; Ferrario, M.; Buda, F. *J. Phys. Chem. B* **2001**, *105*, 4386.

(13) Epifanovsky, E.; Polyakov, I.; Brigorenko, B.; Nemukhin, A.; Krylov, A. I. *J. Chem. Theory Comput.* **2009**, *5*, 1895.

(14) Wan, S. B.; Liu, S. S.; Zhao, G. J.; Chen, M. D.; Han, K. L.; Sun, M. T. *Biophys. Chem.* **2007**, *129*, 218.

(15) Gromov, E. V.; Burghardt, I.; Köppel, H.; Cederbaum, L. S. *J. Am. Chem. Soc.* **2007**, *129*, 6798.

(16) Send, R.; Sundholm, D. *Phys. Chem. Chem. Phys.* **2007**, *9*, 2862.

(17) Ko, C.; Levine, B.; Toniolo, A.; Manohar, L.; Olsen, S.; Werner, H. J.; Martínez, T. J. *J. Am. Chem. Soc.* **2003**, *125*, 12710.

(18) Toniolo, A.; Olsen, S.; Manohar, L.; Martínez, T. J. *Faraday Discuss.* **2004**, *127*, 149.

(19) Cembran, A.; González-Luque, R.; Altoè, P.; Merchán, M.; Bernardi, F.; Olivucci, M.; Garavelli, M. *J. Phys. Chem. A* **2005**, *109*, 6597.

(20) Molina, V.; Merchán, M. *Proc. Natl. Acad. Sci. U.S.A.* **2001**, *98*, 4299.

(21) Martin, M. E.; Negri, F.; Olivucci, M. *J. Am. Chem. Soc.* **2004**, *126*, 5452.

(22) Sekharan, S.; Weingart, O.; Buss, V. *Biophys. J.* **2006**, *91*, L07.

(23) Bravaya, K.; Bochenkova, A.; Granovsky, A.; Nemukhin, A. *J. Am. Chem. Soc.* **2007**, *129*, 13035.

(24) Schautz, F.; Buda, F.; Filippi, C. *J. Chem. Phys.* **2004**, *121*, 5835.

(25) Filippi, C.; Zaccheddu, M.; Buda, F. *J. Chem. Theory Comput.* **2009**, *5*, 2074.

(26) Schreiber, M.; Silva-Junior, M. R.; Sauer, S. P. A.; Thiel, W. *J. Chem. Phys.* **2008**, *128*, 134110.

(27) Andersen, L. H.; Bochenkova, A. V. *Eur. Phys. J. D* **2009**, *51*, 5.

(28) Christiansen, O.; Koch, H.; Jørgensen, P.; Olsen, J. *Chem. Phys. Lett.* **1996**, *256*, 185.

(29) Koch, H.; Christiansen, O.; Jørgensen, P.; Olsen, J. *Chem. Phys. Lett.* **1995**, *244*, 75.

(30) Nemukhin, A. V.; Bochenkova, A. V.; Bravaya, K. B.; Granovsky, A. A. *Proc. SPIE* **2007**, *6449*, 64490N.

(31) Cai, Z. L.; Sendt, K.; Reimers, J. R. *J. Chem. Phys.* **2002**, *117*, 5543.

(32) Dreuw, A.; Head-Gordon, M. *J. Am. Chem. Soc.* **2004**, *126*, 4007.

(33) Hedin, L.; Lundqvist, S. Effects of Electron−Electron and Electron−Phonon Interactions on the One-Electron States of Solids. *Solid State Physics: Advances in Research and Application*; Academic Press: New York, 1969; Vol. 23, pp 1−181.

(34) Onida, G.; Reining, L.; Rubio, A. *Rev. Mod. Phys.* **2002**, *74*, 601.

(35) Rohlfing, M.; Louie, S. G. *Phys. Rev. B* **2000**, *62*, 4927.

(36) Albrecht, S.; Reining, L.; Del Role, R.; Onida, G. *Phys. Rev. Lett.* **1998**, *80*, 4510.

(37) Ma, Y.; Rohlfing, M. *Phys. Rev. B* **2008**, *77*, 115118.

(38) Shirley, E. L. *Phys. Rev. Lett.* **1998**, *80*, 794.

(39) Rohlfing, M.; Louie, S. G. *Phys. Rev. Lett.* **1998**, *80*, 3320.

(40) Artacho, E.; Rohlfing, M.; Côté, M.; Haynes, P. D.; Needs, R. J.; Molteni, C. *Phys. Rev. Lett.* **2004**, *93*, 116401.

(41) Rohlfing, M.; Louie, S. G. *Phys. Rev. Lett.* **1999**, *82*, 1959.

(42) Ismail-Beigi, S.; Louie, S. G. *Phys. Rev. Lett.* **2003**, *90*, 076401.

(43) Tiago, M. L.; Chelikowsky, J. R. *Phys. Rev. B* **2006**, *73*, 205334.

(44) Putschögl, M.; Zirak, P.; Penzkofer, A. *Chem. Phys.* **2008**, *343*, 107.

(45) Creemers, T. M. H.; Lock, A. J.; Subramaniam, V.; Jovin, T. M.; Völker, S. *Nat. Struct. Biol.* **1999**, *6*, 557.

(46) Ryan, W. L.; Gordon, D. J.; Levy, D. H. *J. Am. Chem. Soc.* **2002**, *124*, 6194.

(47) Soler, J. M.; Artacho, E.; Gale, J. D.; García, A.; Junquera, J.; Ordejón, P.; Sánchez-Portal, D. *J. Phys.: Condens. Matter* **2002**, *14*, 2745.

(48) Perdew, J. P.; Burke, K.; Ernzerhof, M. *Phys. Rev. Lett.* **1996**, *77*, 3865.

(49) Troullier, N.; Martins, J. L. *Phys. Rev. B* **1991**, *43*, 1993.

(50) Gromov, E. V.; Burghardt, I.; Köppel, H.; Cederbaum, L. S. *J. Phys. Chem. A* **2005**, *109*, 4623.

(51) Sun, M. T.; Ding, Y.; Cui, G. L.; Liu, Y. J. *J. Phys. Chem. A* **2007**, *111*, 2946.

(52) Wanko, M.; Hoffmann, M.; Strodel, P.; Koslowski, A.; Thiel, W.; Neese, F.; Frauenheim, T.; Elstner, M. *J. Phys. Chem. B* **2005**, *109*, 3606.

(53) Aulbur, W. G.; Jönsson, L.; Wilkins, J. W. Quasiparticle Calculations in Solids. *Solid State Physics: Advances in Research and Application*; Academic Press: New York, 2000; Vol. 54, pp 1−218.

(54) Rohlfing, M.; Krüger, P.; Pollmann, J. *Phys. Rev. B* **1995**, *52*, 1905.

(55) de Groot, M.; Buma, W. J. *J. Phys. Chem. A* **2005**, *109*, 6135.

(56) Hybertsen, M. S.; Louie, S. G. *Phys. Rev. B* **1986**, *34*, 5390.

(57) Li, Q. S.; Fang, W. H. *Chem. Phys.* **2005**, *313*, 71.

(58) Tian, Z. X.; Kass, S. R. *J. Am. Chem. Soc.* **2008**, *130*, 10842.

(59) Tian, Z. X.; Wang, X. B.; Wang, L. S.; Kass, S. R. *J. Am. Chem. Soc.* **2009**, *131*, 1174.

(60) Meyer, T. E. *Biochim. Biophys. Acta* **1985**, *806*, 175.

(61) Devanathan, S.; Pacheco, A.; Ujj, L.; Cusanovich, M.; Tollin, G.; Lin, S.; Woodbury, N. *Biophys. J.* **1999**, *77*, 1017.

(62) Bell, A. F.; He, X.; Wachter, R. M.; Tonge, P. J. *Biochemistry* **2000**, *39*, 4423.

(63) Dong, J.; Solntsev, K. M.; Tolbert, L. M. *J. Am. Chem. Soc.* **2006**, *128*, 12038.

(64) Sinicropi, A.; Andruniow, T.; Ferré, N.; Basosi, R.; Olivucci, M. *J. Am. Chem. Soc.* **2005**, *127*, 11534.

(65) Ma, Y.; Rohlfing, M. Unpublished work (2009).

CT900528H